RESEARCH ARTICLE SUMMARY

PALEOCLIMATE

A 485-million-year history of Earth's surface temperature

Emily J. Judd*, Jessica E. Tierney, Daniel J. Lunt, Isabel P. Montañez, Brian T. Huber, Scott L. Wing, Paul J. Valdes

INTRODUCTION: A long-term geological record of global mean surface temperature (GMST) is important for understanding the history of our planet and putting present-day climate change into context. Such a record is necessary for constraining the relationship between climate and other aspects of the Earth system, including the evolution and extinction of life, and the chemistry of the atmosphere and oceans. Further, quantifying the relationship between GMST and atmospheric carbon dioxide (CO_2) concentrations can refine our understanding of Earth's climate sensitivity and improve future predictions under anthropogenic warming.

RATIONALE: Although several Phanerozoic (the last 539 million years) temperature reconstructions exist, during the intensively studied Cenozoic Era (the last 66 million years), they are colder and less variable than individual estimates from key time periods, particularly during ice-free (greenhouse) intervals. This discrepancy suggests that existing Phanerozoic temperature records may underestimate past temperature change, and merits further investigation using a new approach.

RESULTS: Here, we present PhanDA, a reconstruction of GMST spanning most of the Phanerozoic Eon. PhanDA was created using data assimilation, a method that statistically integrates geological data with climate model simulations. PhanDA indicates that Earth's temperature has varied between 11° and 36°C over the past 485 million years. This range is larger than previous reconstructions; however, PhanDA agrees well with independent GMST estimates from the Cenozoic, providing confidence in its larger dynamical range.

PhanDA reveals key features in the relationship between GMST and the pole-to-equator temperature gradient, including polar amplification (i.e., larger temperature changes at high latitudes) and a shallowing of the gradient with increasing GMST. Tropical temperatures range between 22° and 42°C, refuting the idea of a fixed upper limit on tropical warmth and suggesting that ancient life must have evolved to endure extreme heat. We parse PhanDA into five climate states and find that overall, Earth has spent more time in warmer climate states than cold ones during the Phanerozoic.

There is a strong relationship between PhanDA GMST and CO_2, indicating that CO_2 is the dominant control on Phanerozoic climate. The consistency of this relationship is surprising because on this timescale, we expect solar luminosity to influence climate. We hypothesize that changes in planetary albedo and other greenhouse gases (e.g., methane) helped compensate for the increasing solar luminosity through time. The GMST-CO_2 relationship indicates a notably constant "apparent" Earth system sensitivity (i.e., the temperature response to a doubling of CO_2, including fast and slow feedbacks) of ~8°C, with no detectable dependence on whether the climate is warm or cold.

CONCLUSION: PhanDA provides a statistically robust estimate of GMST through the Phanerozoic. We find that Earth's temperature has varied more dynamically than previously thought and that greenhouse climates were very warm. CO_2 is the dominant driver of Phanerozoic climate, emphasizing the importance of this greenhouse gas in shaping Earth history. The consistency of apparent Earth system sensitivity (~8°C) is surprising and deserves further investigation. More broadly, PhanDA provides critical context for the evolution of life on Earth, as well as present and future climate changes. ■

The list of author affiliations is available in the full article online.
*Corresponding author. Email: ejjudd@syr.edu
Cite this article as E. J. Judd *et al.*, *Science* **385**, eadk3705 (2024). DOI: 10.1126/science.adk3705

READ THE FULL ARTICLE AT
https://doi.org/10.1126/science.adk3705

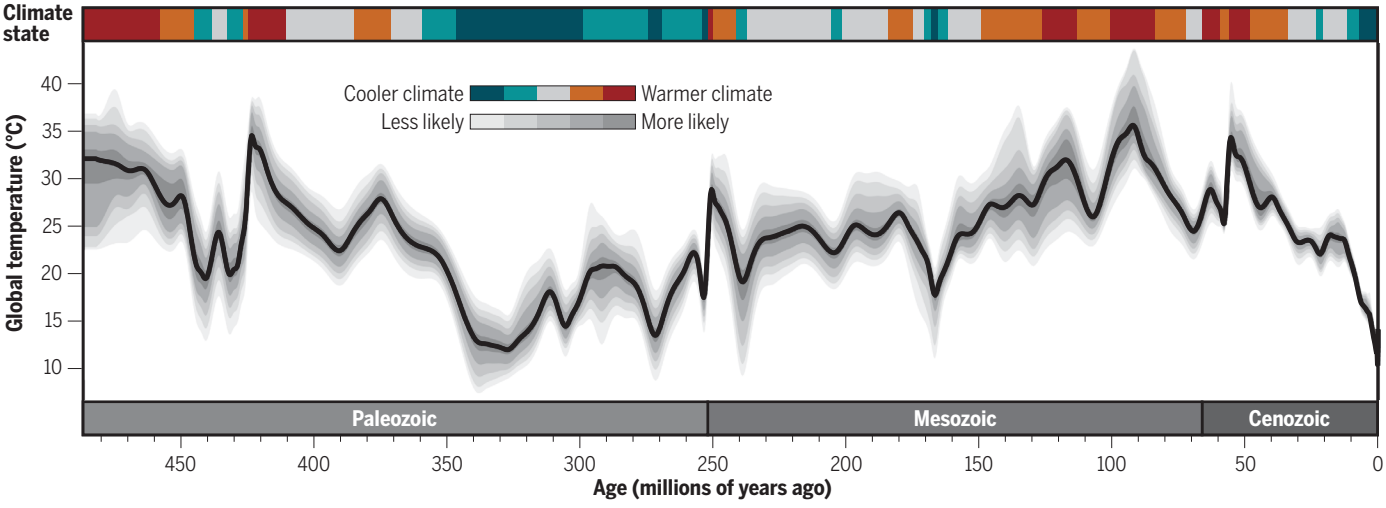

PhanDA global mean surface temperature across the last 485 million years. The gray shading corresponds to different confidence levels, and the black line shows the average solution. The colored bands along the top reflect the climate state, with cooler colors indicating icehouse (coolhouse and coldhouse) climates, warmer colors indicating greenhouse (warmhouse and hothouse) climates, and the gray representing a transitional state.

RESEARCH ARTICLE

PALEOCLIMATE

A 485-million-year history of Earth's surface temperature

Emily J. Judd[1,2]*, Jessica E. Tierney[2], Daniel J. Lunt[3], Isabel P. Montañez[4], Brian T. Huber[1], Scott L. Wing[1], Paul J. Valdes[3,5]

A long-term record of global mean surface temperature (GMST) provides critical insight into the dynamical limits of Earth's climate and the complex feedbacks between temperature and the broader Earth system. Here, we present PhanDA, a reconstruction of GMST over the past 485 million years, generated by statistically integrating proxy data with climate model simulations. PhanDA exhibits a large range of GMST, spanning 11° to 36°C. Partitioning the reconstruction into climate states indicates that more time was spent in warmer rather than colder climates and reveals consistent latitudinal temperature gradients within each state. There is a strong correlation between atmospheric carbon dioxide (CO_2) concentrations and GMST, identifying CO_2 as the dominant control on variations in Phanerozoic global climate and suggesting an apparent Earth system sensitivity of ~8°C.

A record of global mean surface temperature (GMST) across the Phanerozoic Eon is essential for building a holistic history of our planet and making more accurate predictions of future climate change. Across the past half-billion years, changes in global climate are intimately linked with evolutionary patterns of both flora and fauna (*1*), tectonics (*2*, *3*), and the chemistry of the atmosphere and oceans (*4*, *5*). Understanding how Earth's surface temperature has evolved over this interval is therefore critical for constraining the mechanisms and feedbacks that drive long-term global change. The range and distribution of GMST across the Phanerozoic also provide context for ongoing human-caused warming. Similarly, estimates of paleo-GMST are necessary for calculating equilibrium climate sensitivity (ECS) (*6*–*9*) and Earth system sensitivity (ESS) (*10*–*13*)—metrics that are important for predicting the climatic consequences of anthropogenic carbon dioxide (CO_2) emissions (*6*, *7*).

Traditionally, Phanerozoic temperature reconstructions rely on either proxy data (*14*, *15*) or Earth system models (ESMs) (*4*, *16*, *17*). Existing proxy-based reconstructions are either restricted to sea-surface temperature (SST) data (*18*, *19*) or extrapolate GMST by combining the tropical SST record with paleo-Köppen climatic belts (*14*, *15*). However, the heterogeneous spatiotemporal coverage of proxy data can bias estimates of GMST (*8*, *20*, *21*), and the fidelity of both the data and the proxy system assumptions are progressively more uncertain with increasing geologic age. Conversely, calculating GMST from the full-field surface air temperature (SAT) outputs provided by ESMs is straightforward (*4*, *16*, *17*) but requires assumptions about boundary conditions (e.g., greenhouse gas concentrations, ice volume) that are challenging to constrain in deep time. Direct model-based estimates of GMST are also dependent on the climate sensitivity of the ESM (*16*, *17*) and, at times, diverge from geologic evidence (*4*, *16*, *17*). Notably, existing long-term records of Phanerozoic GMST from both proxies (*14*, *15*) and models (*4*, *16*, *17*) tend to show lower temperature variability and overall colder temperatures than independent time slice estimates from the well-studied Cenozoic (*8*, *9*, *22*–*26*), suggesting that the dynamic range of Phanerozoic temperature might be underestimated. These discrepancies raise doubts about our understanding of Earth's long-term climatic history and underscore the need for a reevaluation using a new approach.

Here, we present PhanDA, a state-of-the-art reconstruction of GMST spanning the last 485 million years of Earth history. PhanDA is based on paleoclimate data assimilation (DA), which statistically combines proxy data with ESM simulations to produce a spatially complete reconstruction of SAT (*27*). This approach leverages the strengths of both proxies and models as sources of information, providing an innovative way to explore the temporal and spatial patterns in Earth's climate across the Phanerozoic.

The PhanDA reconstruction

We reconstruct Phanerozoic GMST using an offline ensemble Kalman filter method to assimilate proxy and model information (*27*–*29*). The method has been applied in more recent time intervals to produce time series of global change (*28*, *30*) and to reconstruct conditions during key time slices, including the Last Glacial Maximum (*31*) and the Paleocene-Eocene Thermal Maximum (PETM) (*24*). The DA framework offers several advantages over traditional model- or proxy-only reconstructions. First, the approach simultaneously updates multiple climate fields, regardless of the type of proxy data used, enabling the reconstruction of SAT while using SST proxy data and therefore simplifying the calculation of GMST. Second, because DA uses an ensemble of ESM simulations rather than a single experiment, the results depend less heavily on the model being run at accurate CO_2 values or on the ESM having accurate climate sensitivity. Third, the posterior ensemble can be used to constrain uncertainty. Finally, by documenting all decision-making and providing the scripts to run the DA, the PhanDA reconstruction is fully reproducible and can easily be updated and refined as new proxy data, ESMs, and forward proxy system models become available.

Following the approach of recent DA reconstructions (*30*, *31*), we assimilated geochemical proxies of SST, which were drawn from the PhanSST database (*21*, *29*). We do not assimilate terrestrial temperature proxy information for several reasons. First, a comprehensive compilation of terrestrial SAT data across the Phanerozoic is not available at this time. Second, we lack formal proxy system models for many of the terrestrial proxies (e.g., leaf margin analysis, palynofloral composition) that we can use in the paleo-DA framework. Finally, many terrestrial datasets require accurate paleoaltimetry estimates, which—especially for mountainous regions—are highly uncertain in deep time and unlikely to be correctly represented by the coarse grid of many model simulations. Although the incorporation of terrestrial data would improve DA estimates over land, given that the oceans represent ~70% of Earth's surface, SST data should be sufficiently predictive for estimating GMST.

We assimilated a total of 85 time slices from the base of the Ordovician through the Holocene. Each time slice generally represents a single geochronologic age (i.e., chronostratigraphic stage), though we combined data from adjacent stages during six data-poor intervals (*29*) and separated the PETM [56 million years ago (Ma)] data from the remainder of the Ypresian (56 to 48.07 Ma) owing to the large amount of data available during this well-studied hyperthermal. Proxy data of the same type and at the same location were averaged within each targeted stage, which resulted in a relatively consistent distribution of assimilated data points across time until the Neogene, when the amount of data increases substantially

[1]Department of Paleobiology, Smithsonian National Museum of Natural History, Washington, DC 20560, USA. [2]Department of Geosciences, University of Arizona, Tucson, AZ 85721, USA. [3]School of Geographical Sciences, University of Bristol, Bristol BS8 1SS, UK. [4]Department of Earth and Planetary Sciences, University of California, Davis, Davis, CA 95616, USA. [5]State Key Laboratory of Tibetan Plateau Earth System, Environment and Resources, Institute of Tibetan Plateau Research, Chinese Academy of Sciences, Beijing 100101, China.
*Corresponding author. Email: ejjudd@syr.edu

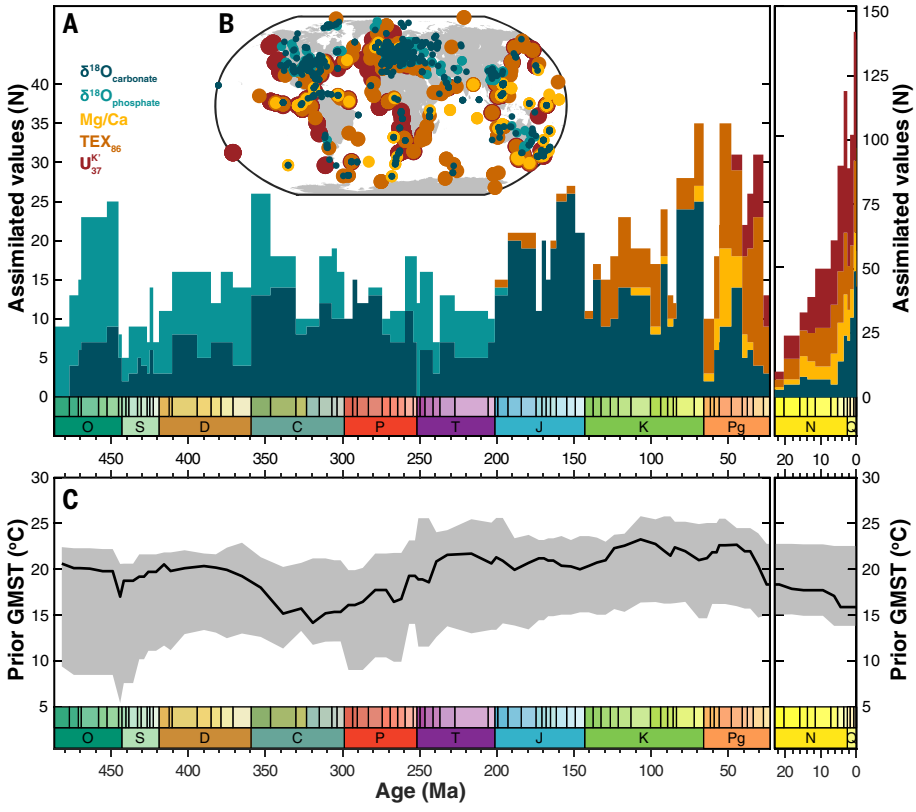

Fig. 1. Proxy and model data used for the PhanDA reconstruction. Temporal (**A**) and spatial (**B**) distribution of stage averaged proxy data used in the assimilation. (**C**) Range (gray band) and median (black line) of GMSTs within the prior model ensemble for each assimilated stage.

(Fig. 1A). We used an 80-member model ensemble for each stage, generated from a collection of over 850 simulations across more than 100 time slices (*29*, *32*), conducted with the fully coupled atmosphere–ocean–vegetation Hadley Centre model, HadCM3L (*33*, *34*). These simulations sample a variety of CO_2 concentrations, paleogeography, and model structural uncertainties and span a broad range of climatic conditions and GMST (Fig. 1B). Our model prior is restricted to HadCM3L output because, as far as we are aware, it is the only set of simulations that provides multiple possible climate solutions through the Phanerozoic [e.g., the CESM model simulations of (*35*) use a single CO_2 trajectory]. We used established forward models to relate the proxy values to climate variables (table S1), accounting for the spatial and temporal variability in seawater $\delta^{18}O$ ($\delta^{18}O_{sw}$), pH, and Mg/Ca values (*29*).

Nearly all proxy data older than the Cretaceous come from oxygen isotope analyses of (both carbonate and phosphate) fossils, and the $\delta^{18}O_{sw}$ is a key assumption inherent to these proxy systems. There is some debate regarding whether or not there has been a long-term secular change in the global average $\delta^{18}O_{sw}$ across the Phanerozoic (*19*, *36*, *37*). The final results shown here sample from two solutions: (i) no secular change, and (ii) a small nonlinear change (i.e., an increase to the baseline "ice-free" value of ~1 per mil (‰) since the Ordovician) induced by Snowball Earth (*37*). We also considered the larger change in $\delta^{18}O_{sw}$ proposed by (*36*) (i.e., an increase of ~5‰ since the Ordovician), but found that applying this assumption resulted in GMST values that, when compared to geological evidence, were unreasonably cold for the majority of the Paleozoic and also yielded a poor correlation with independent clumped isotope temperature estimates (*29*) (fig. S1).

The PhanDA reconstruction is appreciably distinct from the model prior (compare Figs. 1C and 2), illustrating the important insight gained from the assimilation of the proxy data. The time-weighted mean GMST across all assimilated stages (24° ± 5°C, 1σ) is both warmer and more variable than that of the prior ensemble (20° ± 2°C), as well as previous Phanerozoic temperature reconstructions (*4*, *14*–*17*) (fig. S2). However, in the relatively data-rich Cenozoic, PhanDA GMST has a strong, nearly 1:1 correlation with independent time slice GMST estimates derived using a variety of methods (*8*, *22*–*26*, *30*) (fig. S3; correlation coefficient $r = 0.90$). The consensus between PhanDA and previous Cenozoic studies adds confidence to our reconstructed GMST during these data-rich intervals as well as the larger dynamic range of PhanDA as compared to previous Phanerozoic temperature reconstructions (*4*, *14*–*17*).

Phanerozoic temperatures

PhanDA indicates that Earth's temperature has varied between minimum values of 11°C [Late Pleistocene; 129 to 11.7 thousand years ago (ka)] and maximum values of 36°C (Turonian; 93.9 to 89.39 Ma) over the past 485 million years and exhibits key features consistent with our current understanding of Phanerozoic climate (Fig. 2). The reconstruction begins with hot conditions in the early Ordovician that gradually cool into the Hirnantian (445.21 to 443.07 Ma), in line with lithologic evidence of glaciation (*2*) and coincident with the Late Ordovician mass extinction (*38*). Although the median Hirnantian GMST (21°C) is warmer than other intervals with known glaciation, the expansive Gondwanan supercontinent amplified continentality, generating subfreezing temperatures in the mid-to-high latitudes and allowing for extensive ice sheets (supplementary text and fig. S4). Warm conditions in the late Devonian, which peak in the Frasnian (378.9 to 371.1 Ma), align with a period of increased volcanism related to emplacement of the Yakutsk-Vilyui (*39*, *40*) and Kola–Dnieper (*39*) large igneous provinces, as well as the Frasnian–Famennian Biotic Crisis (*38*). The warmth of the Frasnian is followed by consistent long-term cooling into the Carboniferous, with temperatures remaining cool but variable in the Permian. A pulse of warming during the Induan (251.9 to 249.88 Ma), the first stage of the Triassic, immediately follows Siberian Traps volcanism (*40*) and the end-Permian Mass Extinction (*38*). Across the Triassic, Jurassic, and most of the Cretaceous, our reconstruction shows a long-term warming trend that culminates in hothouse conditions during the Turonian, followed by gradual cooling at the close of the Mesozoic Era. Across the Cenozoic, as a whole, GMST closely follows the trajectory of the benthic foraminiferal $\delta^{18}O$ stack (*41*) [fig. S5; $r = -0.96$, $P < 0.01$ (*42*)]. Maximum temperatures are reached during the PETM, an ephemeral hyperthermal associated with a negative carbon isotope excursion (*43*) and emplacement of the North Atlantic Igneous Province (*40*), with warmth sustained into the early Eocene (Ypresian). GMST from the late Paleogene through the Holocene agrees well with the estimates of glacial extent (*2*), which indicate a short-lived retreat of ice sheets during the early Neogene and rapid expansion during the Quaternary.

Despite the general agreement between PhanDA and other records of global change, there are certain times when PhanDA diverges from established patterns. For example, although the overall colder conditions during the Carboniferous and Permian broadly coincide with the

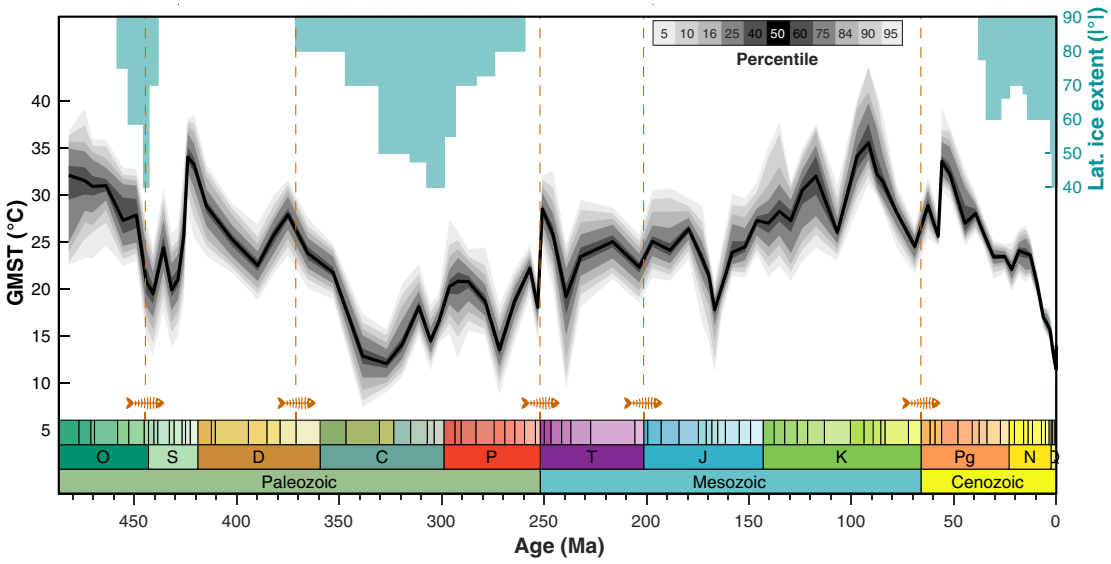

Fig. 2. Phanerozoic temperature history. PhanDA reconstructed GMST for the past 485 million years. Black line shows the median, shading corresponds to the ensemble percentile. Blue rectangles show the maximum latitudinal ice extent (*2*), and orange dashed lines show the timing of the five major mass extinctions of the Phanerozoic (*36*).

timing of the Late Paleozoic Ice Age (LPIA), the minimum GMST occurs earlier (Serpukhovian; 330.34 to 323.4 Ma) than the maxima in glacial occurrence data (*44*) and latitudinal ice extent (*2*) (Kasimovian–Gzhelian; 307.02 to 298.89 Ma). However, glacial occurrence and ice extent records ultimately offer little insight into ice volume. Many of the traditional glacial indicators (e.g., diamictites) can have nonglacial origins (*45*), complicating interpretation of the rock record, and limited outcrop of older rocks and poor age control can make it difficult to discern between isolated alpine glaciers and widespread ice sheets (*45*, *46*). For example, recent work now suggests that Gondwana's spatially diachronous LPIA glacial record reflects the changing locations of depocenters as the continent drifted eastward across the south pole (*45*, *46*). In addition, some of the perceived temporal misalignment is likely related to time averaging of temperature and glacial data across stages that experienced both ice expansion and retreat (*46*). It is also possible that glacial indicators from the LPIA are skewed toward younger stages of the ice age as a consequence of depositional and preservational biases (*47*). Indeed, several lines of evidence suggest an earlier apex in glaciation. There is a global multimillion-year unconformity at the close of the Serpukhovian, coincident with an increase in inferred magnitudes of glacioeustasy (*46*, *48*) and a severe biodiversity crisis (*49*). Further, a recent study finds evidence for sustained deglaciation across a broad swath of southern Gondwana during the latest Carboniferous (*50*), suggesting that the peak of the LPIA must have occurred earlier. The trajectory of GMST presented here agrees well with these revised interpretations of the evolution of the LPIA.

Likewise, although PhanDA shows good agreement with the time slice estimates from the Cenozoic (fig. S3), there is a notable deviation with the benthic foraminiferal oxygen isotope record (*41*) during the middle Miocene (fig. S5C). During the Serravallian (13.82 to 11.63 Ma) and Tortonian (11.63 to 7.25 Ma) stages, PhanDA indicates relatively warm temperatures, but the benthic values are comparatively enriched in ^{18}O. This could suggest that the rise in benthic $\delta^{18}O$ following the middle Miocene Climatic Optimum represents ice sheet growth rather than global cooling. In addition, although GMSTs estimated by scaling the benthic data (*51*) are nearly indistinguishable from PhanDA during the late Neogene and Quaternary, they are systematically offset across the remainder of the Cenozoic (fig. S5C), suggesting that the scaling assumptions used by (*51*) do not fully capture greenhouse temperatures. A large component of this mismatch is likely due to the "pH effect" on the foraminiferal $\delta^{18}O$. Applying the theoretical pH correction (*52*, *53*) to the benthic $\delta^{18}O$ prior to scaling them generates GMST estimates that closely approach a 1:1 relationship with PhanDA (fig. S5D).

Phanerozoic climate states and latitudinal gradients

Earth's climate is generally considered to oscillate between two dominant regimes: icehouse intervals, with unipolar or bipolar continental ice sheets and steep pole-to-equator temperature gradients, and greenhouse intervals, which lack widespread continental ice sheets and exhibit shallow latitudinal temperature gradients (*54*). PhanDA provides an internally consistent, full-field reconstruction, enabling a valuable opportunity to interrogate the temporal variability of climate states (Fig. 3A) and the spatial patterns that define them (Fig. 3D). We rank the median GMST from each stage to form five quantiles, each representing a different climate state (Fig. 3B; "coldhouse," "coolhouse," "transitional," "warmhouse," and "hothouse"). The quantiles are assigned on the basis of GMST alone, making them independent from a priori knowledge of or assumptions about the climate system (e.g., ice volume and atmospheric CO_2 concentrations). Further, the quantiles are assigned at the stage level (which has variable duration) rather than at a fixed time step, which allows them to be used to quantify how much time was spent in each state (Fig. 3C).

The time series of climate states as a whole shows two distinct first-order oscillations between periods of warmth (in the early Paleozoic and late Mesozoic through early Cenozoic) and periods of cold (in the late Paleozoic and late Cenozoic), which are separated by transitional intervals (Fig. 3A). These oscillations mirror long-term cyclicity in other records of global change, such as eustatic sea level, and are most likely driven by the supercontinent cycle (*3*, *15*, *55*). The temporal trends generally follow lithologic evidence for glaciation (*2*, *44*, *46*). During both the LPIA and late Cenozoic glaciations, shifts from warmhouse to transitional states coincide with early occurrences of glacial deposits (Famennian, 371.1 to 359.3 Ma, and Rupelian, 33.9 to 27.29 Ma, respectively) (*2*). Likewise, the transition to sustained coldhouse conditions in the late Cenozoic occurs during the last stage of the Miocene (Messinian; 7.25 to 5.33 Ma), coincident with early evidence of Northern Hemisphere ice-rafted debris (*56*) and evidence for a decline in CO_2 that approaches the proposed threshold for bipolar glaciation (*57*, *58*). Assuming that the coolhouse and coldhouse states collectively represent icehouse regimes, whereas the warmhouse and hothouse states represent greenhouse regimes, then greenhouse climates have been the dominant mode over the past 485 million years, accounting

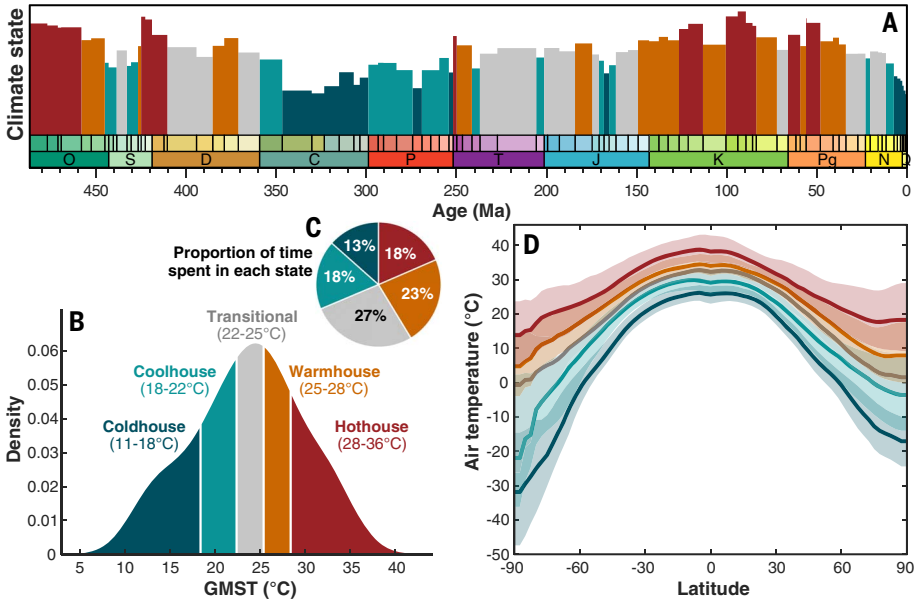

Fig. 3. Climate states across the Phanerozoic. (**A**) Time series of Earth's climate state, with each stage assigned a state in accordance with the quantiles defined in panel (B) and the height of each rectangle scaled by the median GMST of that stage. (**B**) Kernel density plot of the distribution of median GMST values, with each the five quantiles defined (the range of which is indicated in the parentheses below each state's label). (**C**) Pie chart showing the proportion of time spent in each climate state across the Phanerozoic. (**D**) The latitudinal surface air temperature gradient associated with each of the climate states (colored bands showing the 16th to 84th percentiles, colored lines showing the median value).

for 41% of Phanerozoic time, whereas icehouse conditions prevailed 31% of the time (Fig. 3C). Coldhouse states, like our present-day climate, are relatively uncommon during the Phanerozoic (13%).

We identify a time-independent pattern in zonally averaged air temperatures under different climate states (Fig. 3D), implying that GMST within each of the five climate states is achieved through distinct meridional distributions of SAT. Consistent with polar amplification, the change in temperatures between the states is largest in the high latitudes, accompanied by non-negligible differences in tropical temperature (Fig. 3D). This pattern gives rise to a strong negative correlation between GMST and the tropical–polar latitudinal temperature gradient [LTG; $r = -0.90$, $P < 0.01$ (*42*); fig. S6A] (*29*). Although this correlation also exists in the model priors, the range of the LTG in PhanDA is much wider, reflecting the influence of the proxy data (fig. S6, B and C). Across the Phanerozoic, the difference in temperature between the tropics and the poles (ΔT_{lat}) ranges from values of ΔT_{lat} = 30° to 48°C during coldhouse climates, to ΔT_{lat} = 14° to 25°C during hothouse climates (figs. S6A and S7 and table S2). This hothouse ΔT_{lat} value agrees well with the range of SST gradient values reported from the Early Eocene Climatic Optimum (*59*–*61*). In addition, we find that icehouse (coldhouse and coolhouse; ΔT_{lat} = 23° to 48°C) LTGs are both larger and more variable than greenhouse (warmhouse and hothouse; ΔT_{lat} = 14° to 27°C) LTGs, as might be expected from dynamically varying amounts of polar land and sea ice. Small differences in the LTG of stages with similar GMST during icehouse intervals can be attributed to differences in their continental configurations, emphasizing the role that paleogeography (and continentality) plays in determining the latitudinal extent of ice sheet (supplementary text and fig. S4). Over the past 90 Ma, PhanDA indicates a range of ΔT_{lat} = 17° to 48°C. This range is much larger than the recent reconstruction of Gaskell *et al.* (*62*) (ΔT_{lat} = 15° to 28°C). However, that study reports latitudinal gradients in SST, not SAT, and so the reduced range is expected because the SST LTG is suppressed during icehouse climates as ocean temperatures approach the freezing point of seawater. When we compute the SST LTG from PhanDA, we find good agreement with the Gaskell *et al.* study (ΔT_{lat} = 18° to 27°C for the past 90 Ma; ΔT_{lat} = 16° to 30°C for the Phanerozoic; table S2).

The potential for an upper limit on tropical warmth during greenhouse intervals (i.e., a tropical thermostat) has been a matter of long-standing discussion (*63*–*65*). Average tropical SAT from the PhanDA reconstruction are highly variable (fig. S7), ranging from 22° to 31°C (median = 27°C) during icehouse intervals to 32° to 42°C (median = 36°C) during greenhouse intervals. The average tropical SSTs during peak Mesozoic (Turonian; 40°C) and Cenozoic (PETM; 38°C) warmth are in good agreement with previous studies documenting extremely high tropical SSTs during these time intervals (*63*, *66*, *67*). Collectively, these findings dispel the idea that there is a fixed tropical thermostat, consistent with proxy evidence generated in the past decade (*59*, *65*) as well as observations and modeling studies (*64*, *68*).

Because GMST is an area-weighted mean, and ~40% of Earth's surface area is located in the tropics, low-latitude temperatures exert a strong influence on GMST. Hence, the warmest tropical temperatures (~40°C) are associated with high (>30°C) GMSTs. Although the possibility that diagenesis has biased the proxy record toward warmer temperatures cannot be ignored, consistency between the maximum GMST values during the Paleozoic, Mesozoic, and Cenozoic (34°, 36°, and 34°C, respectively)—eras characterized by different dominant proxy systems, depositional environments, and taxa—provides support that the high GMSTs are a real and persistent feature of the Phanerozoic. In addition, our Cenozoic hothouse GMSTs (during the Eocene and PETM) are in good agreement with previous work (*8*, *24*) (fig. S3).

The GMST values reported during hothouse intervals do, however, raise the question of whether some regional temperatures on land may have exceeded the thermal limit for multicellular life. Experiments suggest that most modern organisms have an upper temperature tolerance of ~35° to 40°C (*69*). Plants adapted to hot deserts can actively grow at or slightly above 40°C but show a steep drop in photosynthetic rates above 45°C (*70*), and leaves suffer irreversible damage above ~50°C (*71*). These limits are based on modern organisms that have not experienced selection for survival under higher than modern temperatures in millions of years, so it is possible that during prolonged periods of warmth, organisms evolved adaptations to survive extreme heat stress. Although there is currently no phylogenetic or fossil evidence to support this hypothesis (*71*), physiological and biochemical adaptations to high temperature would be difficult to discern in the fossil record. However, assuming these limits are static through time, during peak hothouse climates, continental temperatures of 45° to 50°C would have been challenging for terrestrial ecosystems.

Ultimately, the potential for terrestrial organisms to withstand extreme heat depends not only upon GMST or mean annual temperature but also on seasonal (and daily) temperatures, as well as humidity, which factors into heat stress (*72*, *73*). PhanDA does not reconstruct these metrics, because doing so reliably would require high-fidelity terrestrial proxy data throughout the Phanerozoic, and PhanDA only assimilates SST proxy data. A thorough investigation of

habitability during the ancient hothouse climates is therefore beyond the scope of this study. However, to get a general sense of the extent of regions with extreme temperatures during hothouse climates, we can turn to the PETM-DA product (*24*). PETM-DA produces a GMST similar to PhanDA (fig. S3; 34°C) but uses a different model prior (simulations conducted with iCESM1.2), assimilates some terrestrial temperature proxy evidence, and is also validated against independent terrestrial temperature data (*24*). The PETM-DA depicts large continental regions where warm mean month temperatures (WMMTs) exceeded 45°C (fig. S8A). However, many extant plants and animals can tolerate extreme heat on a temporary basis (*70*, *74*), so it is also important to consider temperatures during the colder parts of the year. The PETM-DA cold month mean temperatures (CMMT) identify only a few isolated areas where extreme heat persists year-round and that are therefore unlikely to have been habitable (fig. S8B). Additionally, the fragmented paleogeography of the PETM results in multiple regional refugia at higher latitudes and altitudes, and in coastal areas, even within the tropics (supplementary text and figs. S8 and S9). Salient examples of regions of refugia are northwestern South America and India, where PETM-DA yields more moderate temperatures (because reconstructed rainfall rates are high) (*24*) and where high floral and faunal diversity occurred (*75*, *76*). Thus, it is likely that even at GMST values of ~35°C, there remained large regions where ecosystems could have thrived.

Phanerozoic GMST and atmospheric CO_2

Atmospheric CO_2 exerts a dominant control on GMST, both today and in the geologic past (*5*, *77*, *78*). Consistent with this expectation, PhanDA GMST closely tracks reconstructed CO_2 (*29*) over the Phanerozoic (Fig. 4A) and there is a significant positive correlation between (log-transformed) CO_2 and GMST (Fig. 4B; r = 0.72, P < 0.01 (*42*)). This correlation is particularly strong across the Cenozoic (r = 0.97, P< 0.01) where both GMST and paleo-CO_2 data density are greatest, but is also high during the comparably data-poor Paleozoic (r = 0.73, P< 0.01). By contrast, there is no discernible relationship between CO_2 and GMST during the Mesozoic (r = −0.37, P = 0.18). The Mesozoic CO_2 reconstruction uses data from four types of CO_2 proxies, and there is not a clear dominance of one particular proxy system (fig. S10A). However, the Mesozoic is distinct from the Paleozoic and Cenozoic in that it does not include (substantial) coolhouse or coldhouse states, so the range of climate states represented in this era is smaller than the other two. Although the spread of the data mostly overlaps with the overall trend, the compressed CO_2 range (and large uncertainties) makes it difficult to detect a CO_2-GMST relationship (Fig. 4, A and B). The poor relationship also arises from the fact that the reconstructed CO_2 does not increase across the mid-Cretaceous hothouse, a discrepancy that has been noted in previous work (*79*). Although this may represent a true decoupling of CO_2 and GMST, it could also result from an incomplete knowledge of how different proxies encode past CO_2 information (*11*). Further work exploring both the CO_2 and temperature proxies is needed to resolve this "Mesozoic Conundrum."

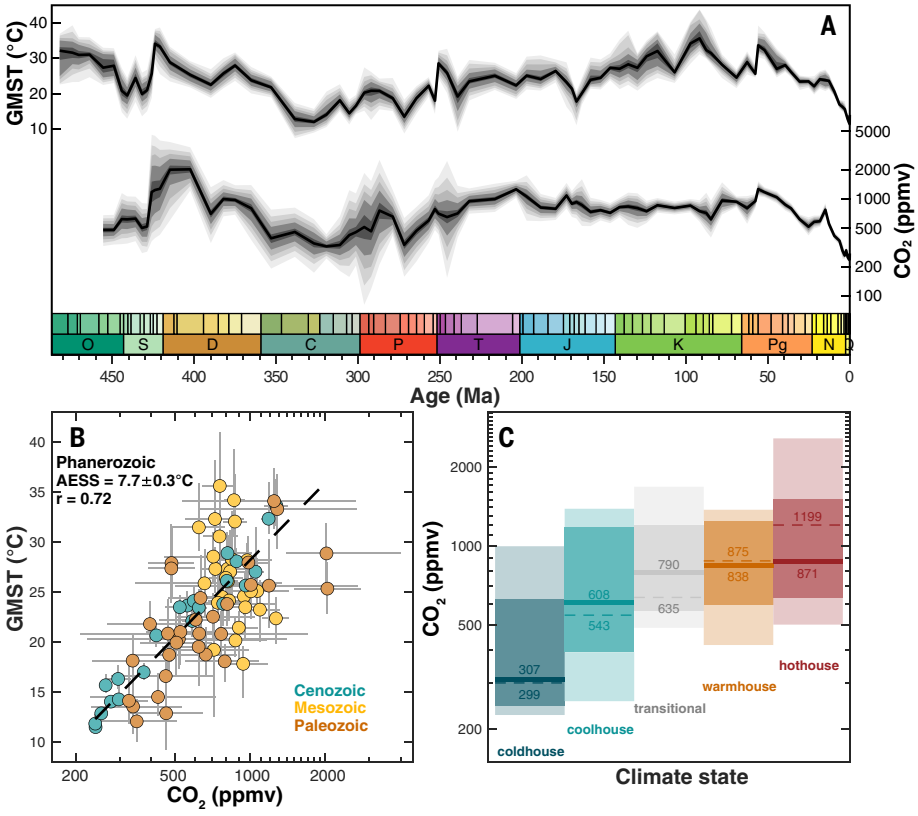

Fig. 4. The relationship between Phanerozoic temperature and atmospheric CO_2. (**A**) PhanDA GMST (top) and reconstructed atmospheric CO_2 (bottom), resolved at the stage level. The CO_2 reconstruction (*29*) is largely based on the data from Foster *et al*. (2017) (*78*) in the Paleozoic and Mesozoic, and the data from Rae *et al*. (2021) (*80*) in the Cenozoic. Shading reflects percentiles, as in Fig. 1. (**B**) PhanDA GMST versus CO_2, color-coded by geologic era. The York regression (*86*), which accounts for uncertainty in both the predictor and response variables, is shown by the black dashed line. (**C**) CO_2 ranges for each of the climate states defined in Fig. 3. Light and dark bands show the 5th to 95th and 16th to 84th percentiles, respectively. The thick solid line shows the median value, and the dashed line shows the median, excluding data from the Mesozoic, where CO_2 is more uncertain.

CO_2 concentrations scale with the climate states defined in Fig. 3 (Fig. 4C), albeit with large ranges related to the uncertainties associated with the CO_2 reconstruction, and real variability in CO_2 and GMST between stages. Notably, the median CO_2 value during coldhouse intervals [307 parts per million by volume (ppmv)] is close to the model-derived threshold for Cenozoic bipolar glaciation (280 ppmv) (*58*), and the median CO_2 value for transitional intervals (790 ppmv) aligns well with the proposed threshold for unipolar glaciation (750 ppmv) (*58*). Although the range is large, median hothouse CO_2 values (871 ppmv) are somewhat low compared to estimates from well-studied greenhouse intervals, such as the early Eocene (~1500 ppmv) (*9*, *80*). This discrepancy is caused by the perplexingly low (~775 ppmv) Cretaceous hothouse CO_2 estimates, despite ample evidence of extreme warmth (*79*). Omitting Mesozoic stages increases the median hothouse CO_2 value to 1199 ppmv, which is in better agreement with the Cenozoic evidence (Fig. 4C).

The consistent relationship between CO_2 and GMST across the record is somewhat surprising given that on Phanerozoic timescales, we expect that non-CO_2 forcings, including changes in solar luminosity and other greenhouse gases, play a role in driving climate change. The ~4.2% increase in solar irradiance since the beginning of the Ordovician (*78*, *81*, *82*) results in an increase in solar forcing (ΔF_{solar}) of ~9.8 W m^{-2}, if planetary albedo (α) is assumed to be constant (*29*). Previous work has

suggested that higher CO_2 compensated for the lower solar luminosity of the early Paleozoic (*78*), yet were that the case, the Paleozoic data should plot far to the right of the Cenozoic data in our cross-plot of CO_2 versus GMST. Instead, the Paleozoic estimates of CO_2, during both greenhouse and icehouse intervals, largely overlap those of the Cenozoic (Fig. 4B). Including the increase in solar irradiance (*29*) degrades the relationship between the change in total forcing (ΔF, relative to preindustrial) and GMST (r = 0.53), and produces ΔF values that are lower than the preindustrial average (i.e., negative) across 84% of the Paleozoic (fig. S11, A and B), despite substantial evidence that global temperatures were warmer than the preindustrial value over much of this time. This creates an enigma wherein the Paleozoic CO_2 values are seemingly too low to compensate for the reduced solar constant. This prominent discrepancy has been noted before in Phanerozoic modeling studies (*4*, *16*) and is independent from the choice of CO_2 reconstruction (e.g., Fig. 2b from Foster *et al*., 2017) (*78*). However, the linear increase in ΔF_{solar} across the Phanerozoic is predicated on the simplifying assumption of a constant planetary albedo. Small changes in α can produce large differences in the net amount of incoming solar radiation to the planet. For example, a linear increase in α over the past 485 million years of just 0.03 fully compensates for the change in solar luminosity (fig. S11C). Planetary albedo is influenced by both atmospheric (e.g., clouds and aerosols) and surface (e.g., the ratio of land to ocean, ice extent, and vegetation cover) albedo (*83*). Most of the factors affecting α are difficult to constrain in deep time; however, one component that is relatively well constrained from plate tectonic reconstructions is the change in the proportion of land to ocean area relative to today (*29*, *84*). The impact of these paleogeographic changes on planetary energy balance can be treated as a forcing (ΔF_{geog}) (*29*, *81*). In the Ordovician, subaerially exposed continents constituted only ~15% of the total surface area of the planet (compared to ~30% today), with the value increasing quasi-linearly across the Paleozoic (fig. S12). This results in an overall lower surface albedo for the Paleozoic and thus a positive forcing. Accounting for ΔF_{geog} improves the correlation with GMST (r = 0.69) by partially offsetting the lower solar irradiance (fig. S11, E and F). However, the correlation is still lower than when just CO_2 forcing is considered, suggesting that either other factors influenced α or that additional forcings helped compensate for the lower solar luminosity. Changes in the concentrations of trace greenhouse gases (e.g., methane, nitrous oxide, and ozone) have almost certainly contributed to Earth's energy balance over various times in the Phanerozoic. For example, modeling studies suggest that the abundant Carboniferous and Permian swamps may have produced more methane (*85*), which could help offset the lower CO_2 and solar forcing during the LPIA. Future work modeling the impact of trace greenhouse gas concentrations and constraining the evolution of albedo across the Phanerozoic will help elucidate the role of non-CO_2 forcing factors and why they appear to be canceled out such that CO_2 is so strongly correlated with GMST.

With CO_2 plotted in $\log_2$ space, the slope of the linear regression between CO_2 and GMST indicates a change in GMST of 7.7° ± 0.3°C per doubling of CO_2 (1σ; based on York regression (*86*), which accounts for errors in both CO_2 and GMST). This value is consistent across the Cenozoic (8.2° ± 0.4°C; fig. S13A), the Paleozoic (7.8° ± 1.5°C; fig. S12B), and the Cenozoic and Paleozoic combined (8.0° ± 0.4°C; fig. S12C). We call this metric, which quantifies the long-term response of GMST to CO_2, the "apparent" Earth system sensitivity (AESS). Like traditional ESS (*10*), AESS includes both fast (e.g., clouds and sea ice) and slow (e.g., ice sheet growth and decay) climate feedbacks. However, it also implicitly assumes that the impact of changes in solar luminosity, paleogeography, non-CO_2 greenhouse gases, or other forcings compensate for each other in some way (as explored above). For these reasons, AESS is not comparable with conventional ECS, which the IPCC AR6 reports is 2° to 5°C for the modern climate (*7*). However, the PhanDA AESS value agrees well with (and is more directly comparable to) CO_2-only ESS estimates spanning the past 10 million years (also 8°C) (*11*) and the past 800 thousand years (7° to 13°C) (*12*, *13*). Unlike some modeling studies, which have indicated that climate sensitivity increases at higher GMST (*61*, *81*, *87*), we do not observe a statistically robust state dependency in AESS in either the Cenozoic or Paleozoic, at least on the stage level. Further work is needed to understand why the AESS value is so consistent across the Phanerozoic, and what determines its ~8°C magnitude.

Conclusions

Data assimilation leverages paleotemperature proxy information and model simulations, capitalizing on both a large catalog of geological data as well as our best physical understanding of Phanerozoic climates (Fig. 1). The resulting product, PhanDA, is a statistically robust and internally consistent reconstruction of GMST spanning the past 485 million years and indicates that Earth's temperature has varied more dynamically than previously thought (Fig. 2). We divide the record into five quantiles, or climate states (Fig. 3), and use these distinctions to demonstrate that, independent of time and throughout the Phanerozoic, GMSTs within each climate state are associated with similar LTGs. In addition to the expected polar amplification, PhanDA indicates a large range in tropical temperatures between the five climate states (22° to 42°C).

PhanDA GMST exhibits a strong relationship with atmospheric CO_2 concentrations (Fig. 4), demonstrating that CO_2 has been the dominant forcing controlling global climate variations across the Phanerozoic. However, because solar luminosity has also changed through time, the relationship is rather enigmatic; long-term changes in planetary albedo or changes in trace greenhouse gas concentrations may help to resolve the discrepancy. The CO_2–GMST relationship also indicates a relatively consistent AESS of ~8°C across the Phanerozoic. This suggests that Phanerozoic GMST is highly predictable on multimillion-year timescales if CO_2 concentrations are known, but that our understanding of how forcings and feedbacks on deep timescales balance—or enhance—one another is incomplete.

Methods summary

The PhanDA data assimilation uses an offline ensemble square root Kalman filter method, implemented in MATLAB using the code package DASH v4.2.1 (*27*). Briefly, an ensemble of posterior states (X_{post}) is calculated from (i) an ensemble of prior states from ESM simulations (X_{prior}); (ii) proxy data (Y_{obs}); (iii) estimated proxy values (Y_{est}), which are forward modeled from the ensemble of prior states; and (iv) the Kalman filter (K). These variables are related using the generalized equation:

$$X_{post} = X_{prior} + K(Y_{obs} - Y_{est}) \quad (1)$$

Details about each of these variables and how they were assembled can be found in the supplementary materials (*29*). In summary, the ESM simulations used in X_{prior} come from the fully coupled atmosphere–ocean–vegetation Hadley Centre model, HadCM3L (*33, 34*), and the proxy data used in Y_{obs} were drawn from the PhanSST database (*21*), which contains over 150,000 proxy estimates from five geochemical proxy systems for SST. We calculated Y_{est}, or the predicted proxy values, from our model priors using established forward models (table S1), accounting for the spatial and temporal variability in the seawater $\delta^{18}O$, pH, and Mg/Ca values. The Kalman gain, K:

$$K = cov(X_{prior}, Y_{est}) \times [cov(Y_{est}, Y_{est}) + R]^{-1} \quad (2)$$

weights and spreads the new information gained through the addition of the proxy data using the covariance (cov) between the prior state and climate variance at the location of the proxy, the covariance of the proxy estimates, and the uncertainty of the proxy values themselves (R). We used data assimilation to reconstructed global conditions at 85 time

slices across the Phanerozoic, which broadly correspond with the geochronologic ages (i.e., chronostratigraphic stages). To better sample the uncertainties related to the choice of prior ensemble (X_{prior}), the seawater chemistry assumptions required to calculate Y_{est}, and the proxy uncertainty (R), each stage was assimilated 420 times, iterating through all permutations of the different scenarios. Some subsets of model priors yield unrealistic results (e.g., unrealistically steep high latitudinal temperature gradients); we created an automated screening protocol to flag and remove these assimilations. The median and uncertainty of the GMST of each time slice was then calculated using the area-weighted mean SAT from the unflagged X_{post} ensembles.

A full description of the methods used in the data assimilation, the determination of the latitudinal temperature gradients and climate states, the construction of the atmospheric CO_2 record, and the estimation of climate forcings across the Phanerozoic can be found in the supplementary materials (*29*).

REFERENCES AND NOTES

1. P. J. Mayhew, M. A. Bell, T. G. Benton, A. J. McGowan, Biodiversity tracks temperature over time. *Proc. Natl. Acad. Sci. U.S.A.* **109**, 15141–15145 (2012). doi: 10.1073/pnas.1200844109; pmid: 22949697
2. F. A. Macdonald, N. L. Swanson-Hysell, Y. Park, L. Lisiecki, O. Jagoutz, Arc-continent collisions in the tropics set Earth's climate state. *Science* **364**, 181–184 (2019). doi: 10.1126/science.aav5300; pmid: 30872536
3. R. D. Nance, The supercontinent cycle and Earth's long-term climate. *Ann. N. Y. Acad. Sci.* **1515**, 33–49 (2022). doi: 10.1111/nyas.14849; pmid: 35762733
4. B. J. Mills, Y. Donnadieu, Y. Godderis, Spatial continuous integration of Phanerozoic global biogeochemistry and climate. *Gondwana Res.* **100**, 73–86 (2021). doi: 10.1016/j.gr.2021.02.011
5. D. L. Royer, R. A. Berner, I. P. Montañez, N. J. Tabor, D. J. Beerling, CO_2 as a primary driver of Phanerozoic climate. *GSA Today* **14**, 4 (2004). doi: 10.1130/1052-5173(2004)014<4:CAAPDO>2.0.CO;2
6. S. C. Sherwood *et al*., An Assessment of Earth's Climate Sensitivity Using Multiple Lines of Evidence. *Rev. Geophys.* **58**, RG000678 (2020). doi: 10.1029/2019RG000678; pmid: 33015673
7. P. Forster *et al*., "The Earth's Energy Budget, Climate Feedbacks, and Climate Sensitivity" in *Climate Change 2021: The Physical Science Basis. Contribution of Working Group I to the Sixth Assessment Report of the Intergovernmental Panel on Climate Change*, V. Masson-Delmotte *et al*., Eds. (Cambridge Univ. Press, 2021), pp. 923–1054.
8. G. N. Inglis *et al*., Global mean surface temperature and climate sensitivity of the early Eocene Climatic Optimum (EECO), Paleocene–Eocene Thermal Maximum (PETM), and latest Paleocene. *Clim. Past* **16**, 1953–1968 (2020). doi: 10.5194/cp-16-1953-2020
9. E. Anagnostou *et al*., Proxy evidence for state-dependence of climate sensitivity in the Eocene greenhouse. *Nat. Commun.* **11**, 4436 (2020). doi: 10.1038/s41467-020-17887-x; pmid: 32895377
10. D. J. Lunt *et al*., Earth system sensitivity inferred from Pliocene modelling and data. *Nat. Geosci.* **3**, 60–64 (2010). doi: 10.1038/ngeo706
11. Cenozoic CO_2 Proxy Integration Project ($CenCO_2PIP$) Consortium, Toward a Cenozoic history of atmospheric CO_2. *Science* **382**, eadi5177 (2023). doi: 10.1126/science.adi5177; pmid: 38060645
12. PALAEOSENS Project Members, Making sense of palaeoclimate sensitivity. *Nature* **491**, 683–691 (2012). doi: 10.1038/nature11574; pmid: 23192145
13. C. W. Snyder, Evolution of global temperature over the past two million years. *Nature* **538**, 226–228 (2016). doi: 10.1038/nature19798; pmid: 27669024
14. C. R. Scotese, H. Song, B. J. Mills, D. G. van der Meer, Phanerozoic paleotemperatures: The earth's changing climate during the last 540 million years. *Earth Sci. Rev.* **215**, 103503 (2021). doi: 10.1016/j.earscirev.2021.103503
15. D. G. van der Meer *et al*., Long-term Phanerozoic global mean sea level: Insights from strontium isotope variations and estimates of continental glaciation. *Gondwana Res.* **111**, 103–121 (2022). doi: 10.1016/j.gr.2022.07.014
16. P. J. Valdes, C. R. Scotese, D. J. Lunt, Deep ocean temperatures through time. *Clim. Past* **17**, 1483–1506 (2021). doi: 10.5194/cp-17-1483-2021
17. T. E. Wong, Y. Cui, D. L. Royer, K. Keller, A tighter constraint on Earth-system sensitivity from long-term temperature and carbon-cycle observations. *Nat. Commun.* **12**, 3173 (2021). doi: 10.1038/s41467-021-23543-9; pmid: 34039993
18. H. Song, P. B. Wignall, H. Song, X. Dai, D. Chu, Seawater Temperature and Dissolved Oxygen over the Past 500 Million Years. *J. Earth Sci.* **30**, 236–243 (2019). doi: 10.1007/s12583-018-1002-2
19. E. L. Grossman, M. M. Joachimski, Ocean temperatures through the Phanerozoic reassessed. *Sci. Rep.* **12**, 8938 (2022). doi: 10.1038/s41598-022-11493-1; pmid: 35624298
20. E. J. Judd, T. Bhattacharya, L. C. Ivany, A Dynamical Framework for Interpreting Ancient Sea Surface Temperatures. *Geophys. Res. Lett.* **47**, e2020GL089044 (2020). doi: 10.1029/2020GL089044
21. E. J. Judd *et al*., The PhanSST global database of Phanerozoic sea surface temperature proxy data. *Sci. Data* **9**, 753 (2022). doi: 10.1038/s41597-022-01826-0; pmid: 36473868
22. C. L. O'Brien *et al*., The enigma of Oligocene climate and global surface temperature evolution. *Proc. Natl. Acad. Sci. U.S.A.* **117**, 25302–25309 (2020). doi: 10.1073/pnas.2003914117; pmid: 32989142
23. N. J. Burls *et al*., Simulating Miocene Warmth: Insights From an Opportunistic Multi-Model Ensemble (MioMIP1). *Paleoceanogr. Paleoclimatol.* **36**, e2020PA004054 (2021). doi: 10.1029/2020PA004054
24. J. E. Tierney *et al*., Spatial patterns of climate change across the Paleocene-Eocene Thermal Maximum. *Proc. Natl. Acad. Sci. U.S.A.* **119**, e2205326119 (2022). doi: 10.1073/pnas.2205326119; pmid: 36215472
25. S. Ring, S. Mutz, T. Ehlers, Cenozoic Proxy Constraints on Earth System Sensitivity to Greenhouse Gases. *Paleoceanogr. Paleoclimatol.* **37**, e2021PA004364 (2022). doi: 10.1029/2021PA004364
26. K. Eichenseer, L. A. Jones, Bayesian multi-proxy reconstruction of early Eocene latitudinal temperature gradients. *Clim. Past* **20**, 349–362 (2024). doi: 10.5194/cp-20-349-2024
27. J. M. King, J. Tierney, M. Osman, E. J. Judd, K. J. Anchukaitis, DASH: a MATLAB toolbox for paleoclimate data assimilation**.** *Geosci. Model Dev.* **16**, 5653–5683 (2023). doi: 10.5194/gmd-16-5653-2023
28. R. Tardif *et al*., Last Millennium Reanalysis with an expanded proxy database and seasonal proxy modeling. *Clim. Past* **15**, 1251–1273 (2019). doi: 10.5194/cp-15-1251-2019
29. Materials and methods are available as supplementary materials.
30. M. B. Osman *et al*., Globally resolved surface temperatures since the Last Glacial Maximum. *Nature* **599**, 239–244 (2021). doi: 10.1038/s41586-021-03984-4; pmid: 34759364
31. J. E. Tierney *et al*., Glacial cooling and climate sensitivity revisited. *Nature* **584**, 569–573 (2020). doi: 10.1038/s41586-020-2617-x; pmid: 32848226
32. E. J. Judd, J. E. Tierney, D. J. Lunt, I. P. Montanez, B. T. Huber, S. L. Wing, P. J. Valdes, PhanDA HadCM3L Model Priors, Version 1 [Data set], Zenodo (2023). https://doi.org/10.5281/zenodo.8237751.
33. V. Pope, M. Gallani, P. Rowntree, R. Stratton, The impact of new physical parametrizations in the Hadley Centre climate model: HadAM3. *Clim. Dyn.* **16**, 123–146 (2000). doi: 10.1007/s003820050009
34. C. Gordon *et al*., The simulation of SST, sea ice extents and ocean heat transports in a version of the Hadley Centre coupled model without flux adjustments. *Clim. Dyn.* **16**, 147–168 (2000). doi: 10.1007/s003820050010
35. X. Li *et al*., A high-resolution climate simulation dataset for the past 540 million years. *Sci. Data* **9**, 371 (2022). doi: 10.1038/s41597-022-01490-4; pmid: 35764652
36. J. Veizer, A. Prokoph, Temperatures and oxygen isotopic composition of Phanerozoic oceans. *Earth Sci. Rev.* **146**, 92–104 (2015). doi: 10.1016/j.earscirev.2015.03.008
37. W. F. Defliese, The impact of Snowball Earth glaciation on ocean water δ 18 O values. *Earth Planet. Sci. Lett.* **554**, 116661 (2021). doi: 10.1016/j.epsl.2020.116661
38. D. M. Raup, J. J. Sepkoski Jr., Mass extinctions in the marine fossil record. *Science* **215**, 1501–1503 (1982). doi: 10.1126/science.215.4539.1501; pmid: 17788674
39. R. E. Ernst, S. A. Rodygin, O. M. Grinev, Age correlation of Large Igneous Provinces with Devonian biotic crises. *Global Planet. Change* **185**, 103097 (2020). doi: 10.1016/j.gloplacha.2019.103097
40. Q. Jiang, F. Jourdan, H. K. Olierook, R. E. Merle, An appraisal of the ages of Phanerozoic large igneous provinces. *Earth Sci. Rev.* **237**, 104314 (2023). doi: 10.1016/j.earscirev.2023.104314
41. T. Westerhold *et al*., An astronomically dated record of Earth's climate and its predictability over the last 66 million years. *Science* **369**, 1383–1387 (2020). doi: 10.1126/science.aba6853; pmid: 32913105
42. W. Ebisuzaki, A Method to Estimate the Statistical Significance of a Correlation When the Data Are Serially Correlated. *J. Clim.* **10**, 2147–2153 (1997). doi: 10.1175/1520-0442(1997)010<2147:AMTETS>2.0.CO;2
43. F. A. McInerney, S. L. Wing, The Paleocene-Eocene Thermal Maximum: A Perturbation of Carbon Cycle, Climate, and Biosphere with Implications for the Future. *Annu. Rev. Earth Planet. Sci.* **39**, 489–516 (2011). doi: 10.1146/annurev-earth-040610-133431
44. G. S. Soreghan, M. J. Soreghan, N. G. Heavens, Explosive volcanism as a key driver of the late Paleozoic ice age. *Geology* **47**, 600–604 (2019). doi: 10.1130/G46349.1
45. J. L. Isbell *et al*., Evaluation of physical and chemical proxies used to interpret past glaciations with a focus on the late Paleozoic Ice Age. *Earth Sci. Rev.* **221**, 103756 (2021). doi: 10.1016/j.earscirev.2021.103756
46. I. P. Montañez, Current synthesis of the penultimate icehouse and its imprint on the Upper Devonian through Permian stratigraphic record. *Spec. Publ. Geol. Soc. Lond.* **512**, 213–245 (2022). doi: 10.1144/SP512-2021-124
47. G. González-Bonorino, N.Eyles, Inverse relation between ice extent and the late Paleozoic glacial record of Gondwana. *Geology* **23**, 1015 (1995). doi: 10.1130/0091-7613(1995)023<1015:IRBIEA>2.3.CO;2
48. M. C. Rygel, C. R. Fielding, T. D. Frank, L. P. Birgenheier, The Magnitude of Late Paleozoic Glacioeustatic Fluctuations: A Synthesis. *J. Sediment. Res.* **78**, 500–511 (2008). doi: 10.2110/jsr.2008.058
49. G. R. McGhee Jr., P. M. Sheehan, D. J. Bottjer, M. L. Droser, Ecological ranking of Phanerozoic biodiversity crises: The Serpukhovian (early Carboniferous) crisis had a greater ecological impact than the end-Ordovician. *Geology* **40**, 147–150 (2012). doi: 10.1130/G32679.1
50. N. Griffis *et al*., A Carboniferous apex for the late Paleozoic icehouse. *Spec. Publ. Geol. Soc. Lond.* **535**, 117–129 (2023). doi: 10.1144/SP535-2022-256
51. J. E. Hansen *et al*., Global warming in the pipeline. *Oxford Open. Clim. Change* **3**, kgad008 (2023). doi: 10.1093/oxfclm/kgad008
52. R. E. Zeebe, An explanation of the effect of seawater carbonate concentration on foraminiferal oxygen isotopes. *Geochim. Cosmochim. Acta* **63**, 2001–2007 (1999). doi: 10.1016/S0016-7037(99)00091-5
53. D. Evans, J. Brugger, G. N. Inglis, P. Valdes, The Temperature of the Deep Ocean Is a Robust Proxy for Global Mean Surface Temperature During the Cenozoic. *Paleoceanogr. Paleoclimatol.* **39**, e2023PA004788 (2024). doi: 10.1029/2023PA004788
54. A. G. Fischer, "Long-term climate oscillations recorded in stratigraphy" in *Climate in Earth History: Studies in Geophysics* (National Academies Press, 1982). pp. 97–104.
55. C. M. Marcilly, T. H. Torsvik, C. P. Conrad, Global Phanerozoic sea levels from paleogeographic flooding maps. *Gondwana Res.* **110**, 128–142 (2022). doi: 10.1016/j.gr.2022.05.011
56. H. C. Larsen *et al*., Seven million years of glaciation in greenland. *Science* **264**, 952–955 (1994). doi: 10.1126/science.264.5161.952; pmid: 17830083
57. R. M. Brown, T. B. Chalk, A. J. Crocker, P. A. Wilson, G. L. Foster, Late Miocene cooling coupled to carbon dioxide with Pleistocene-like climate sensitivity. *Nat. Geosci.* **15**, 664–670 (2022). doi: 10.1038/s41561-022-00982-7
58. R. M. Deconto *et al*., Thresholds for Cenozoic bipolar glaciation. *Nature* **455**, 652–656 (2008). doi: 10.1038/nature07337; pmid: 18833277
59. M. J. Cramwinckel *et al*., Synchronous tropical and polar temperature evolution in the Eocene. *Nature* **559**, 382–386 (2018). doi: 10.1038/s41586-018-0272-2; pmid: 29967546

60. D. J. Lunt *et al*., DeepMIP: Model intercomparison of early Eocene climatic optimum (EECO) large-scale climate features and comparison with proxy data. *Clim. Past* **17**, 203–227 (2021). doi: 10.5194/cp-17-203-2021
61. J. Zhu, C. J. Poulsen, J. E. Tierney, Simulation of Eocene extreme warmth and high climate sensitivity through cloud feedbacks. *Sci. Adv.* **5**, eaax1874 (2019). doi: 10.1126/sciadv.aax1874; pmid: 31555736
62. D. E. Gaskell *et al*., The latitudinal temperature gradient and its climate dependence as inferred from foraminiferal $\delta^{18}O$ over the past 95 million years. *Proc. Natl. Acad. Sci. U.S.A.* **119**, e2111332119 (2022). doi: 10.1073/pnas.2111332119; pmid: 35254906
63. P. N. Pearson *et al*., Warm tropical sea surface temperatures in the Late Cretaceous and Eocene epochs. *Nature* **413**, 481–487 (2001). doi: 10.1038/35097000; pmid: 11586350
64. I. N. Williams, R. T. Pierrehumbert, M. Huber, Global warming, convective threshold and false thermostats. *Geophys. Res. Lett.* **36**, 2009GL039849 (2009). doi: 10.1029/2009GL039849
65. C. L. O'Brien *et al*., High sea surface temperatures in tropical warm pools during the Pliocene. *Nat. Geosci.* **7**, 606–611 (2014). doi: 10.1038/ngeo2194
66. K. L. Bice *et al*., A multiple proxy and model study of Cretaceous upper ocean temperatures and atmospheric CO_2 concentrations. *Paleoceanography* **21**, 2005PA001203 (2006). doi: 10.1029/2005PA001203
67. T. Aze *et al*., Extreme warming of tropical waters during the Paleocene–Eocene Thermal Maximum. *Geology* **42**, 739–742 (2014). doi: 10.1130/G35637.1
68. R. Fu, A. D. D. Genio, W. B. Rossow, W. Timothy Liu, Cirrus-cloud thermostat for tropical sea surface temperatures tested using satellite data. *Nature* **358**, 394 (1992). doi: 10.1038/358394a0
69. J. M. Bennett *et al*., GlobTherm, a global database on thermal tolerances for aquatic and terrestrial organisms. *Sci. Data* **5**, 180022 (2018). doi: 10.1038/sdata.2018.22; pmid: 29533392
70. J. Berry, O. Bjorkman, Photosynthetic Response and Adaptation to Temperature in Higher Plants. *Annu. Rev. Plant Physiol.* **31**, 491–543 (1980). doi: 10.1146/annurev.pp.31.060180.002423
71. M. Slot *et al*., Leaf heat tolerance of 147 tropical forest species varies with elevation and leaf functional traits, but not with phylogeny. *Plant Cell Environ.* **44**, 2414–2427 (2021). doi: 10.1111/pce.14060; pmid: 33817813
72. S. C. Sherwood, M. Huber, An adaptability limit to climate change due to heat stress. *Proc. Natl. Acad. Sci. U.S.A.* **107**, 9552–9555 (2010). doi: 10.1073/pnas.0913352107; pmid: 20439769
73. A. Farnsworth *et al*., Climate extremes likely to drive land mammal extinction during next supercontinent assembly. *Nat. Geosci.* **16**, 901–908 (2023). doi: 10.1038/s41561-023-01259-3
74. G. J. Tattersall *et al*., Coping with thermal challenges: Physiological adaptations to environmental temperatures. doi: 10.1002/cphy.c110055; pmid: 23723035
75. C. Jaramillo, M. J. Rueda, G. Mora, Cenozoic plant diversity in the neotropics. *Science* **311**, 1893–1896 (2006). doi: 10.1126/science.1121380; pmid: 16574860
76. J. Rust *et al*., Biogeographic and evolutionary implications of a diverse paleobiota in amber from the early Eocene of India. *Proc. Natl. Acad. Sci. U.S.A.* **107**, 18360–18365 (2010). doi: 10.1073/pnas.1007407107; pmid: 20974929
77. S. Arrhenius, XXXI. *On the influence of carbonic acid in the air upon the temperature of the ground. Lond. Edinb. Dublin Philos. Mag. J. Sci.* **41**, 237–276 (1896). doi: 10.1080/14786449608620846
78. G. L. Foster, D. L. Royer, D. J. Lunt, Future climate forcing potentially without precedent in the last 420 million years. *Nat. Commun.* **8**, 14845 (2017). doi: 10.1038/ncomms14845; pmid: 28375201
79. B. T. Huber, K. G. MacLeod, D. K. Watkins, M. F. Coffin, The rise and fall of the Cretaceous Hot Greenhouse climate. *Global Planet. Change* **167**, 1–23 (2018). doi: 10.1016/j.gloplacha.2018.04.004
80. J. W. Rae *et al*., Atmospheric CO_2 over the Past 66 Million Years from Marine Archives. *Annu. Rev. Earth Planet. Sci.* **49**, 609–641 (2021). doi: 10.1146/annurev-earth-082420-063026
81. A. Farnsworth *et al*., Climate Sensitivity on Geological Timescales Controlled by Nonlinear Feedbacks and Ocean Circulation. *Geophys. Res. Lett.* **46**, 9880–9889 (2019). doi: 10.1029/2019GL083574
82. D. Gough, Solar interior structure and luminosity variations. *Sol. Phys.* **74**, 21–34 (1981). doi: 10.1007/BF00151270
83. A. Donohoe, D. S. Battisti, Atmospheric and Surface Contributions to Planetary Albedo. *J. Clim.* **24**, 4402–4418 (2011). doi: 10.1175/2011JCLI3946.1
84. C. M. Marcilly, T. H. Torsvik, M. Domeier, D. L. Royer, New paleogeographic and degassing parameters for long-term carbon cycle models. *Gondwana Res.* **97**, 176–203 (2021). doi: 10.1016/j.gr.2021.05.016
85. O. Bartdorff, K. Wallmann, M. Latif, V. Semenov, Phanerozoic evolution of atmospheric methane. *Global Biogeochem. Cycles* **22**, 2007GB002985 (2008). doi: 10.1029/2007GB002985
86. D. York, N. M. Evensen, M. L. Martínez, J. De Basabe Delgado, Unified equations for the slope, intercept, and standard errors of the best straight line. *Am. J. Phys.* **72**, 367–375 (2004). doi: 10.1119/1.1632486
87. R. Caballero, M. Huber, State-dependent climate sensitivity in past warm climates and its implications for future climate projections. *Proc. Natl. Acad. Sci. U.S.A.* **110**, 14162–14167 (2013). doi: 10.1073/pnas.1303365110; pmid: 23918397

ACKNOWLEDGMENTS

The climate model simulations were carried out using the computational facilities of the Advanced Computing Research Centre, University of Bristol (https://www.bristol.ac.uk/acrc). **Funding:** E.J.J. was supported by the PhanTASTIC Postdoctoral Fellowship, funded by Roland and Debra Sauermann through the Smithsonian Institution. Additional support was provided by J.E.T. from grant 2016-015 from the Heising-Simons Foundation and the Thomas R. Brown Distinguished Chair in Integrative Science. D.J.L. and P.J.V. acknowledge support from NERC project NE/X000222/1; PaleoGradPhan: Paleoclimate meridional and zonal gradients in the Phanerozoic. **Author contributions:** All others contributed to the conceptualization of the work presented. B.T.H. and S.L.W. secured the initial funding. D.J.L. and P.J.V. ran the climate model simulations, and E.J.J. and J.E.T. built the proxy database. E.J.J. ran the assimilations and produced the results and figures. E.J.J. and J.E.T. wrote the initial manuscript and all authors reviewed and edited it. **Competing interests:** The authors have no competing interests to declare. **Data and materials availability:** Both the model priors (*32*) and the proxy data (*21*) necessary to reproduce the results are publicly available on Zenodo (*32*). The code to run the assimilation and generate the manuscript figures, as well as files containing the GMST, CO_2, and LTG values presented in this paper, are available on GitHub (https://github.com/EJJudd/PhanDA). **License information:**

SUPPLEMENTARY MATERIALS

science.org/doi/10.1126/science.adk3705
Materials and Methods
Supplementary Text
Figs. S1 to S20
Tables S1 to S3
References (*88*–*131*)

Submitted 21 August 2023; accepted 25 July 2024
10.1126/science.adk3705